Dissecting the Mechanism of Epac Activation via Hydrogen−Deuterium Exchange FT-IR and Structural Modeling†

Shaoning Yu,‡,§ Fenghui Fan,‖ Samuel C. Flores,⊥ Fang Mei,‖ and Xiaodong Cheng*,‡,‖

Department of Pharmacology and Toxicology and Sealy Center for Structural Biology, The University of Texas Medical Branch, Galveston, Texas 77555-1031, and Department of Physics, Yale University, P.O. Box 208120, New Haven, Connecticut 06520-8120

Received August 20, 2006; Revised Manuscript Received October 12, 2006

ABSTRACT: Exchange proteins directly activated by cAMP (Epac) make up a family of cAMP binding domain-containing proteins that play important roles in mediating the effects of cAMP through the activation of downstream small GTPases, Ras-proximate proteins. To delineate the mechanism of Epac activation, we probed the conformation and structural dynamics of Epac using amide hydrogen−deuterium (H−D) exchange coupled with Fourier transform infrared spectroscopy (FT-IR) and structural modeling. Our studies show that unlike that of cAMP-dependent protein kinase (PKA), the classic intracellular cAMP receptor, binding of cAMP to Epac does not induce significant changes in overall secondary structure and structural dynamics, as measured by FT-IR and the rate of H−D exchange, respectively. These results suggest that Epac activation does not involve significant changes in the amount of exposed surface areas as in the case of PKA activation, and conformational changes induced by cAMP in Epac are most likely confined to small local regions. Homology modeling and comparative structural analyses of the CBDs of Epac and PKA lead us to propose a model of Epac activation. On the basis of our model, Epac activation by cAMP employs the same underlying structural principal utilized by PKA, although the detailed structural and conformational changes associated with Epac and PKA activation are significantly different. In addition, we predict that during Epac activation the first β-strand of the switchboard switches its conformation to a α-helix, which folds back to the β-barrel core of the CBD and interacts directly with cAMP to form the base of the cAMP-binding pocket.

Exchange proteins directly activated by cAMP (Epac)[1] and cAMP-dependent protein kinase (PKA) are two cAMP receptors that mediate the intracellular actions of the second messenger cyclic AMP in eukaryotic cells. While PKA phosphorylates multiple downstream substrates, Epac proteins act as guanine nucleotide exchange factors (GEFs) for the small GTP-binding proteins Rap1 and Rap2. The discovery of Epac proteins in 1998 as the second family of intracellular cAMP receptors (*1*, *2*) has opened a new chapter in the studies of cAMP-mediated signaling as Epac proteins have been implicated in a myriad of cAMP-related cellular functions, such as exocytosis (*3*−*5*), cell adhesion (*6*, *7*), cell−cell junction (*8*, *9*), and differentiation (*10*). Furthermore, Epac and PKA have been shown to exert synergistic or antagonistic effects on downstream signaling targets depending upon the specific cellular contexts (*11*, *12*). The existence of two highly coordinated cAMP effectors therefore provides a mechanism for a more precise and integrated control of the cAMP signaling pathways in a spatial and temporal manner (*13*).

Both Epac and PKA are regulated by a cAMP binding domain (CBD) that is evolutionarily conserved to the CBD of the bacterial transcriptional factor, cAMP receptor protein. CBD, the only common structural module between PKA and Epac, acts as a molecular switch for sensing the intracellular second messenger cAMP levels. In the case of PKA, the regulatory (R) and catalytic (C) components of PKA are encoded as two separated polypeptides. Binding of cAMP to the tandem CBDs of the R subunit induces a conformational change that leads to dissociation of the holoenzyme (R_2C_2) and subsequent activation of PKA (*14*). X-ray crystal structures of the PKA holoenzyme complex and individual subunits reveal a molecular mechanism for cAMP-mediated activation of PKA (*15*−*17*). The R and C subunits form a large interface in the PKA holoenzyme complex with several key residues (Tyr247 and Trp196) of the C subunit binding directly to the phosphate binding cassette (PBC) of CBD-A

† This work is supported by a grant from the National Institutes of Health (GM060170).

* To whom correspondence should be addressed: Department of Pharmacology and Toxicology, The University of Texas Medical Branch, 301 University Blvd., Galveston, TX 77555-1031. Telephone: (409) 772-9656. Fax: (409) 772-9642. E-mail: xcheng@utmb.edu.

‡ Sealy Center for Structural Biology, The University of Texas Medical Branch.

§ Current address: Fudan University, Shanghai, China.

‖ Department of Pharmacology and Toxicology, The University of Texas Medical Branch.

⊥ Yale University.

[1] Abbreviations: cAMP, cyclic adenosine 3′,5′-monophosphate; CBD, cAMP binding domain; Epac, exchange protein directly activated by cAMP; DEP, Dishevelled, Egl-10, Pleckstrin domain; FT-IR, Fourier transform infrared; GEF, guanine nucleotide exchange factor; PBC, phosphate-binding cassette; PBS, phosphate-buffered saline; PKA, cAMP-dependent protein kinase; C, catalytic subunit of PKA; R, regulatory subunit of PKA; RA, Ras association domain; Rap, Ras-proximate; REM, Ras exchange motif.

10.1021/bi061701x CCC: $33.50
Published on Web 12/05/2006

in the R subunit (*17*). cAMP not only competes directly with the C subunit for these interactions but also induces major conformational changes in the R subunit, particularly the helical subdomain of CBD, the inhibitor sequence and the linker region (*16*, *17*). These conformational changes lead to the reorientation and displacement of the inhibitor sequence from the active site cleft of C and, consequently, the activation of PKA. On the other hand, the CBD in Epac is covalently connected to the catalytic GEF domain as a single polypeptide chain and the intramolecular interaction between the CBD and GEF domains sterically blocks the access of downstream effector Rap. Recently, the crystal structure of Epac2 is determined in the absence of cAMP (*18*). In this autoinhibited Epac2 structure, the second CBD of Epac2, which is common in Epac1 and Epac2, is loosely connected to the CDC-25 homology guanine nucleotide exchange (GEF) domain by the central "switchboard" and an ionic "latch" (*18*). Unlike the extensive interface between the R and C subunits of the PKA holoenzyme, the intramolecular interaction between the regulatory and catalytic regions in Epac2 is surprisingly brief, suggesting that the detailed mechanisms of activation of PKA and Epac by cAMP will most likely be different at the structural level.

In an earlier study, we probed the conformation states of PKA holoenzyme complexes using amide hydrogen−deuterium (H−D) exchange Fourier transform infrared spectroscopy (FT-IR) and chemical protein footprinting (*19*). Consistent with the crystal structure study of the PKA holoenzyme complex, significant conformational changes were observed during PKA activation. In addition, binding of cAMP to PKA holoenzymes leads to a downshift in the IR wavenumber for both the α-helix and β-strand bands, suggesting that R and C subunits become overall more dynamic in the holoenzyme complexes (*19*). Since the structure of Epac in its active state is not currently available, the molecular mechanism of Epac activation is not known. In this study, we investigated the conformational and dynamic states of Epac1 in the presence and absence of cAMP using H−D exchange FT-IR and structural modeling to delineate the mechanism of Epac activation.

EXPERIMENTAL PROCEDURES

Protein Expression and Purification. Δ(1−148)Epac1 was expressed as a GST fusion protein (pGEX4T2) in *Escherichia coli* and purified as described previously (*20*). Briefly, *E. coli* BL21-DE3 cells carrying the Δ(1−148)Epac1 expression vector were grown in LB medium containing 100 μg/mL ampicillin at 37 °C. Protein expression was induced with 100 μM IPTG at room temperature for 9 h after A_{600} reached 0.8−1.2. Cells were harvested, resuspended in PBS buffer with 10% (v/v) glycerol, 1 mM EDTA, 5 mM DTT, and 1 mM PMSF, and lysed using a sonicator. After centrifugation, the supernatant was loaded onto a pre-equilibrated GSH column (Pharmacia). The column was washed sequentially with (1) 360 mM NaCl in PBS, (2) 50 mM Tris-HCl (pH 7.6), 100 mM KCl, 10 mM $MgCl_2$, 10% glycerol, 5 mM DTT, and 2 mM ATP, and (3) 50 mM Tris-HCl (pH 7.6), 50 mM NaCl, 10% glycerol, and 5 mM DTT. The GST−Δ(1−148)Epac1 fusion protein that eluted from the column was cleaved with 150 units of immobilized thrombin for 3 h at 4 °C to remove the GST tag. After the removal of immobilized thrombin beads by centrifugation, Δ(1−148)-Epac1 was further purified by gel filtration on Superdex 200 in buffer A containing 50 mM Tris-HCl (pH 7.6), 50 mM NaCl, 5% glycerol, and 5 mM DTT. Purified proteins were judged to be at least 95% pure by SDS−polyacrylamide gel electrophoresis.

FT-IR Spectroscopy. FT-IR spectra were recorded with a Bomem (Quebec City, PQ) MB series Fourier transform infrared spectrometer equipped with a dTGS detector and purged constantly with dry air. Protein samples (∼15 mg/mL) were warmed to room temperature and loaded in a CaF_2 cell with a 7.5 μm spacer. For each spectrum, a 256-scan interferogram was collected in single-beam mode with a 4 cm^{-1} resolution at a rate of three scans per second. Reference spectra were recorded under identical conditions with only the corresponding buffer in the cell. Protein spectra were recorded using a previously established protocol (*21*). A straight baseline between 2000 and 1750 cm^{-1} was used as the standard for judging the success of water subtraction. Second-derivative spectra were obtained with a seven-point Savitsky−Golay derivative function, baseline-corrected, and area-normalized as described previously (*21*). The secondary structure content of Δ(1−148)Epac1 was calculated by curve fitting analysis of the inverted second-derivative spectrum in the amide I band range from 1600 to 1700 cm^{-1} (*22*). This band is ascribed to >C═O stretching vibration of the peptide bond (*23*). It was assumed that the fraction of residues composing each secondary structural element is proportional to the relative percent area of the associated vibrational band (*24*, *25*).

Hydrogen−Deuterium Exchange Measurement. Protein (100 μL) in buffer A was lyophilized at room temperature to dryness. There was no significant difference in the catalytic activity and the contents of α-helices and β-sheets between the lyophilized (after rehydration) and unlyophilized proteins measured by FT-IR. Samples for H−D exchange experiments were prepared by dissolving the lyophilized 100 μL of Δ-(1−148)Epac1 or buffer solution with or without 300 μM cAMP in the same volume of D_2O. The reconstituted sample was injected immediately into an IR cell with a path length of 50 μm. One minute after the addition of D_2O, single-beam spectra were recorded using kinetic scanning mode. FT-IR spectra were recorded at 1, 2, 3, 4, 5, 6, 7, 8, 9, 10, 11, 15, 20, 30, 40, 50, 60, 90, 120, 150, and 180 min in D_2O. Eight scans were collected for each time interval between 1 and 10 min, while 64 and 128 scans were used for each time interval between 11 and 90 min and longer, respectively. To compare the FT-IR spectra in H_2O and D_2O, we normalized the amide I band in H_2O to the amide I band in D_2O at 1 min. The spectrum collected after exchange for 24 h was used as the fully deuterated spectrum.

Calculation of the Amide Proton Exchange Rate. We monitored the H−D exchange of Epac1 by following apparent intensity changes of the amide II band, located around 1548 cm^{-1}, that is attributed to a combination of N−H in-plane bending and C−N stretching vibrations in the peptide bond, because this band does not adversely interfere with absorption bands of H_2O, HOD, or D_2O (*24*). As the N−H bond in protein is exchanged for a N−D bond in D_2O, the absorption peak of N−D bending vibration at ∼1450 cm^{-1} is strengthened while the magnitude of the N−H absorption peak is decreased. The fraction of unexchanged

amide proton, *F*, was calculated at various time intervals using eq 1:

$$F = (A_{II} - A_{II\infty})/A_I\omega \quad (1)$$

where A_I and A_{II} are the absorbance maxima of the amide I and II bands, respectively, $A_{II\infty}$ is the amide II absorbance maximum of fully deuterated protein, and ω is the ratio of A_{IIo}/A_{Io}, with A_{IIo} and A_{Io} being the absorbance maxima for the amide II and amide I bands, respectively, of Δ(1−148)Epac1 in H_2O (*26*).

The exchange kinetic parameters were fitted with eq 2:

$$F = A_1e^{-k_1t} + A_2e^{-k_2t} + C \quad (2)$$

where *F* is the amide proton fraction at time *t*, k_1 and k_2 are the intermediate and slow exchange rates, respectively, and A_1, A_2, and *C* are constants.

Structural Modeling of Epac1. The Epac1 structural model is initially generated using homology modeling software MODELLER (*27*; http://www.salilab.org/modeller/). The recently determined Epac2 three-dimensional coordinates (2BYV) (*18*) were used as the template. The initial Epac1 model was further refined using the molecular dynamics simulation package GROMACS (http://www.gromacs.org/) to obtain the final Epac1 model.

RESULTS

FT-IR Spectra of Δ(1−148)Epac1 in a H_2O Solution. We used Δ(1−148)Epac1 in this study as published literature so far indicates that the function of the 148 N-terminal residues is mainly associated with cellular targeting of Epac1 in vivo (*28*, *29*), which is further supported by extensive biophysical and biochemical characterization by Wittinghofer and colleagues showing that Δ(1−148)Epac1 retains all measurable biochemical properties such as cAMP binding and Rap activation (*30*). Removal of the first 148 residues significantly improves Epac1 solubility and increases expression levels in *E. coli*, while the full-length Epac1 protein cannot be expressed and purified in sufficient quantity (ref *31* and unpublished data). The FT-IR absorption spectra of Δ(1−148)Epac1 in the presence and absence of 300 μM cAMP in buffer A are shown in Figure 1A. The second-derivative amide I spectra of Δ(1−148)-Epac1 (Figure 1B) all exhibited basic band components that can be assigned to secondary structure components. Quantitative analysis of the secondary structure of Δ(1−148)-Epac1 by curve fitting revealed that Δ(1−148)Epac1 contained 65% α-helices, 14% β-strands, and 21% β-turns (Figure 2A and Table 1). Binding of cAMP to Δ(1−148)-Epac1 did not lead to significant changes in FT-IR second-derivative spectra and overall secondary structure (Figure 2B and Table 1).

H−D Exchanges of Δ(1−148)Epac1 Monitored by FT-IR. To explore the intrinsic protein dynamics and conformational flexibility of Epac1, H−D exchange of Δ(1−148)Epac1 were monitored by FT-IR. Figure 3A shows an overlay of the representative absorption spectra of Δ(1−148)Epac1 recorded at 1, 3, 5, 10, 30, 60, 120, and 180 min in D_2O with spectra of the proteins in H_2O and fully deuterated in D_2O plotted as references. While the Δ(1−148)Epac1 spectra in H_2O exhibited characteristic amide I and II band maxima at 1652 and 1548 cm^{-1}, respectively, H−D exchange in D_2O led to a time-dependent isotopic shift of the amide II band from 1548 to 1455 cm^{-1}. This effect is indicative of NH to ND exchange of peptide

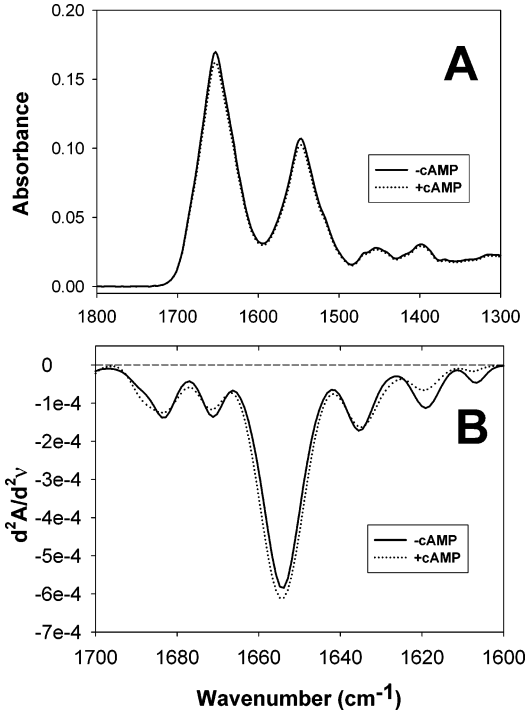

FIGURE 1: FT-IR spectra of Epac1 in the absence and presence of cAMP. (A) IR absorption spectra of Δ(1−148)Epac1 in the absence (—) and presence (···) of 300 μM cAMP. (B) Secondary-derivative amide I spectra of Δ(1−148)Epac1 in the absence (—) and presence (···) of 300 μM cAMP.

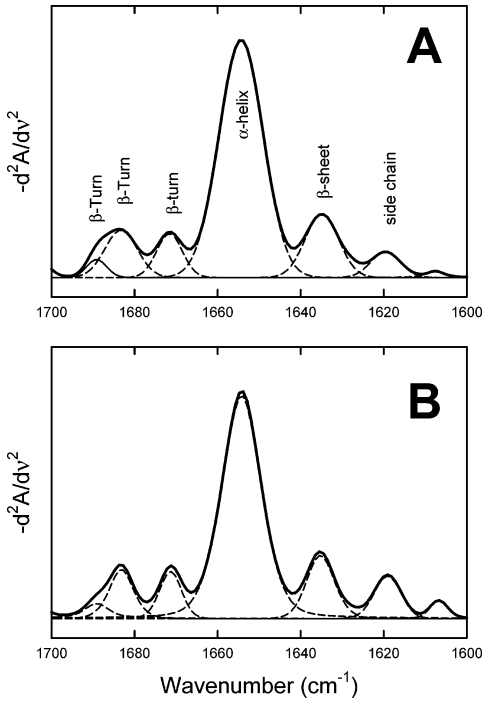

FIGURE 2: Calculation of secondary structural components of Δ(1−148)Epac1 holoenzymes. Deconvolution of inverted secondary-derivative amide I spectra of Δ(1−148)Epac1 in the absence (A) and presence (B) of 300 μM cAMP. Secondary structure contents were obtained from curve fitting of the second-derivative FT-IR spectra using a seven-point Savitsky−Golay derivative function.

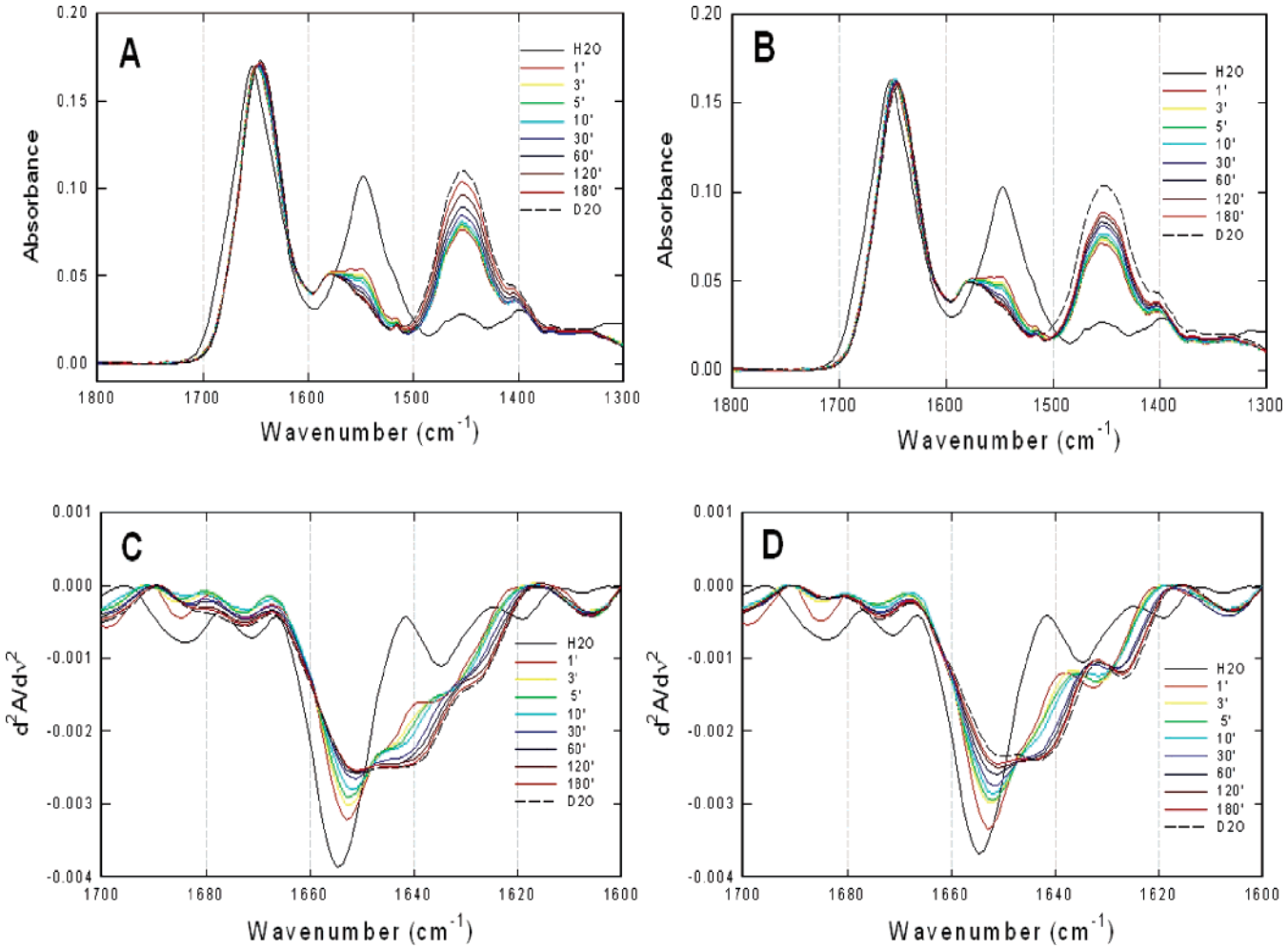

FIGURE 3: H−D exchange of Epac1 as monitored by FT-IR spectroscopy. Infrared spectra of Δ(1−148)Epac1 in the absence (A) and presence (B) of 300 μM cAMP at various time intervals after being dissolved in D_2O at room temperature. Secondary-derivative amide I spectra of Δ(1−148)Epac1 in the absence (C) and presence (D) of 300 μM cAMP at various time intervals after being dissolved in D_2O at room temperature. The spectra of proteins in H_2O and in D_2O after exchange for 24 h drawn as solid and dashed lines, respectively, were included for comparison.

backbone groups that causes a downshift of approximately 100 cm^{-1} in the vibrational frequency of the amide II band (*32*).

To dissect the overlapping band components of the amide I region, second-derivative analyses were performed. Figure 3C shows an overlay of second-derivative spectra of Δ(1−148)Epac1 as a function of H−D exchange time. Almost immediately after the proteins are dissolved in D_2O, the 1655 cm^{-1} band in the α-helix spectral region o f Δ(1−148)Epac1 underwent an initial large drop in intensity and 2 cm^{-1} downshift to 1653 cm^{-1} at the 1 min time measurement, followed by a gradual intensity decrease and a downshift to 1651 cm^{-1} accompanied by a shoulder around 1646 cm^{-1}. The downshift and decrease in intensity of the 1655 cm^{-1} band were completed in ~60 min. On the other hand, the effects of deuterium exchange on the β-sheet spectral region were different. The 1634.5 cm^{-1} β-sheet band increased in intensity initially at the 1 min time measurement, followed by a gradual downshift to form a shoulder around 1629 cm^{-1} in D_2O (Figure 3C).

H−D Exchanges of Δ(1−148)Epac1 in the Presence of cAMP. The overall H−D exchange absorption profiles of Δ(1−148)Epac1 in the presence of cAMP were very similar to those in the absence of cAMP (Figure 3A,B). The secondary derivative spectra of Δ(1−148)Epac1 H−D exchange in the presence of cAMP were also similar but with noticeable differences (Figure 3C,D). Unlike the spectral shifts in the absence of cAMP, the downshift and decrease

Table 1: Secondary Structure Contents of Δ(1−148)Epac1 Determined by FT-IR[a]

Δ(1−148)Epac1			Δ(1−148)Epac1 with 300 μM cAMP		
frequency (cm^{-1})	percent	assignment	frequency (cm^{-1})	percent	assignment
1690.1−1684.3	11.9 ± 0.4	β-turn	1689.1−1683.7	12.1 ± 1.2	β-turn
1671.4 ± 0.2	8.8 ± 2.0	β-turn	1671.2 ± 0.4	6.9 ± 0.1	β-turn
1654.2 ± 0.1	65.4 ± 0.3	α-helix	1654.2 ± 0.1	66.8 ± 1.1	α-helix
1634.5 ± 0.3	13.9 ± 2.5	β-strand	1634.9 ± 0.4	14.2 ± 2.9	β-strand

[a] Secondary structure contents were obtained from curve fitting of the second-derivative FT-IR spectra using a seven-point Savitsky−Golay derivative function as shown in Figure 2.

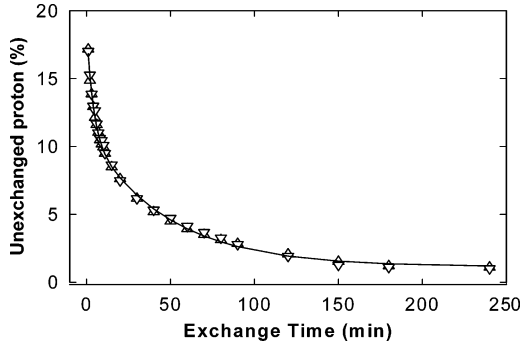

FIGURE 4: Amide proton exchange rates of Epac1. Fraction of unexchanged amide protons as a function of exposure time in D_2O for Δ(1−148)Epac1 in the absence (△) and presence (▽) of 300 μM cAMP. The lines represent best fits to the data points using a two-exponential function as described in eq 2.

in intensity of the 1655 cm^{-1} band were slower and were not complete after 180 min. In addition, the 1655 cm^{-1} band was downshifted by 5 cm^{-1} in the presence of cAMP instead of 4 cm^{-1} as observed in the absence of cAMP, and the shoulder around 1646 cm^{-1} observed in the absence of cAMP became much more prominent in the presence of cAMP to form a noticeable peak at 1643 cm^{-1}. Like that of Δ(1−148)Epac1 in the absence of cAMP, the 1634.5 cm^{-1} β-sheet band also increased in intensity initially at the 1 min time measurement followed by a gradual downshift as in the absence of cAMP. However, instead of a shoulder around 1629 cm^{-1}, a distinct peak at 1627 cm^{-1} was observed for fully deuterated Δ(1−148)Epac1 in the presence of cAMP.

Differences in Overall H−D Exchange between Δ(1−148)-Epac1 and cAMP-Bound Δ(1−148)Epac1. The overall H−D exchange rates of Δ(1−148)Epac1 in the absence and presence of cAMP were estimated by plotting the fraction of unexchanged amide protons, calculated from amide II band data using eq 1, as a function of time. In general, all amide protons in proteins can be divided into three classes (*33*−*35*): (1) fast exchange protons, which are most likely located on the surface of the protein or in regions that are easily solvent accessible, (2) amide protons with intermediate rates located in flexible buried regions, and (3) the slow exchange fraction located in the core region of the protein. The fraction of the unexchanged amide protons at the first exchange time point (1 min) for Δ(1−148)Epac1 in the absence and presence of cAMP was around 20% as shown in Figure 4, suggesting that the majority of the amide protons exchanged so rapidly that their exchange was completed within the time interval of the acquisition of the first time point. Therefore, only the intermediate and slow exchange protons can be practically monitored semiquantitatively over the time range employed in this study. A two-exponential decay model (eq 2) was used to describe the exchange reaction of the remaining amide protons within the experimental time frame, and the resolved parameters are summarized in Table 2. Because of the complexity of the overall H−D exchange reaction in protein, no attempt was made to quantitatively associate these parameters with any actual physical properties; instead, they were only used qualitatively to assess the overall dynamics of Δ(1−148)Epac1 in the absence and presence of cAMP. Overall, there are no significant differences in H−D exchange rates between active and inactive Epac1 states (Table 2 and Figure 4).

Table 2: Fitted Exchange Parameters for Δ(1−148)Epac1[a]

parameter[b]	Δ(1−148)Epac1	Δ(1−148)Epac1 with cAMP
A_1	8.0 ± 0.3	7.9 ± 0.3
A_2	9.6 ± 0.3	9.9 ± 0.3
k_1 (min^{-1})	0.21 ± 0.02	0.26 ± 0.02
k_2 (min^{-1})	0.02 ± 0.01	0.02 ± 0.01
c	0.8 ± 0.2	1.3 ± 0.1
F_0 (%)	17.02	17.17

[a] Parameters were derived from fitting the exchange data in Figure 4 to a two-exponential model as described by eq 2. [b] k_1 and k_2 are the intermediate and slow exchange rates, respectively. A_1, A_2, and C are the constants, while F_0 is the remaining amide proton fraction after D_2O exposure for 1 min.

Structural Modeling of Epac1. Recently, the three-dimensional structure of Epac2 in its cAMP-free, inactive state have been determined (*18*). Since Epac1 is more than 50% identical to Epac2 in amino acid sequence, we constructed an Epac1 three-dimensional model based on the crystal structure of Epac2 using homology modeling (Figure 5A). The final model of Epac1 has a Ramachandran *Z*-score of −0.572, which is similar to that of the Epac2 template structure (−0.411). Because of the extensive sequence homology between Epac1 and -2, the three-dimensional model of Epac1 should be reliable for further structural analysis. It is not surprising that the overall structural architecture of Epac1 is almost identical to the crystal structure of Epac2. Important contact points between the catalytic core and regulatory regions revealed by the Epac2 structure are also preserved in the Epac1 model. For example, the three-stand β-sheet formed by the C-terminus of CBD and the N-terminus of the REM domain interacts with the loop of the helical hairpin of the catalytic core through an extensive hydrogen bonding network to form the switchboard (Figure 5B), while the second helix of the hairpin is anchored by Phe797 and Ile785, which forms a hydrophobic core with the two helices of the REM domain (Figure 5C). Like Epac2, there is only one brief contact point between the CBD and the catalytic core of Epac1. However, the detailed molecular interactions for this specific contact point are different between Epac1 and -2. While the hydrogen bonding between Asp750 (Asp863 in Epac2) of the catalytic core and Gln168 (Gln303 in Epac2) of the CBD is preserved, the Arg886 residue that interacts with Asp307 and Glu332 in Epac2 is replaced with a tryptophan in Epac1 (Figure 5D). Ionic interactions between Arg886 and Asp307 and between Arg886 and Glu332 in Epac2 are substituted by potential hydrogen bonding between Trp753 and His200 and between Trp753 and Gln168, as well as ionic interactions between Arg756 and Asp196 in Epac1 (Figure 5D).

Mechanism of Epac Activation. Our amide H−D exchange and FT-IR studies suggest that activation of Epac by cAMP likely involves local motion, such as hinge movements. Therefore, we subjected the Epac1 model to further structural analysis using the HingeMaster server, which predicts hinge locations in single protein structures using algorithm combines FlexOracle, TLSMD, StoneHinge, and NSHP hinge predictors for maximum accuracy (*36*) [The Yale Morph Server (http://molmovdb.org)]. Our analysis revealed a major hinge in Epac1 between residues 310 and 345 (Figure 6A). This region has been identified as the "lid" region at the C-terminus of CBD that plays an important role in the communication between the regulatory and catalytic domains

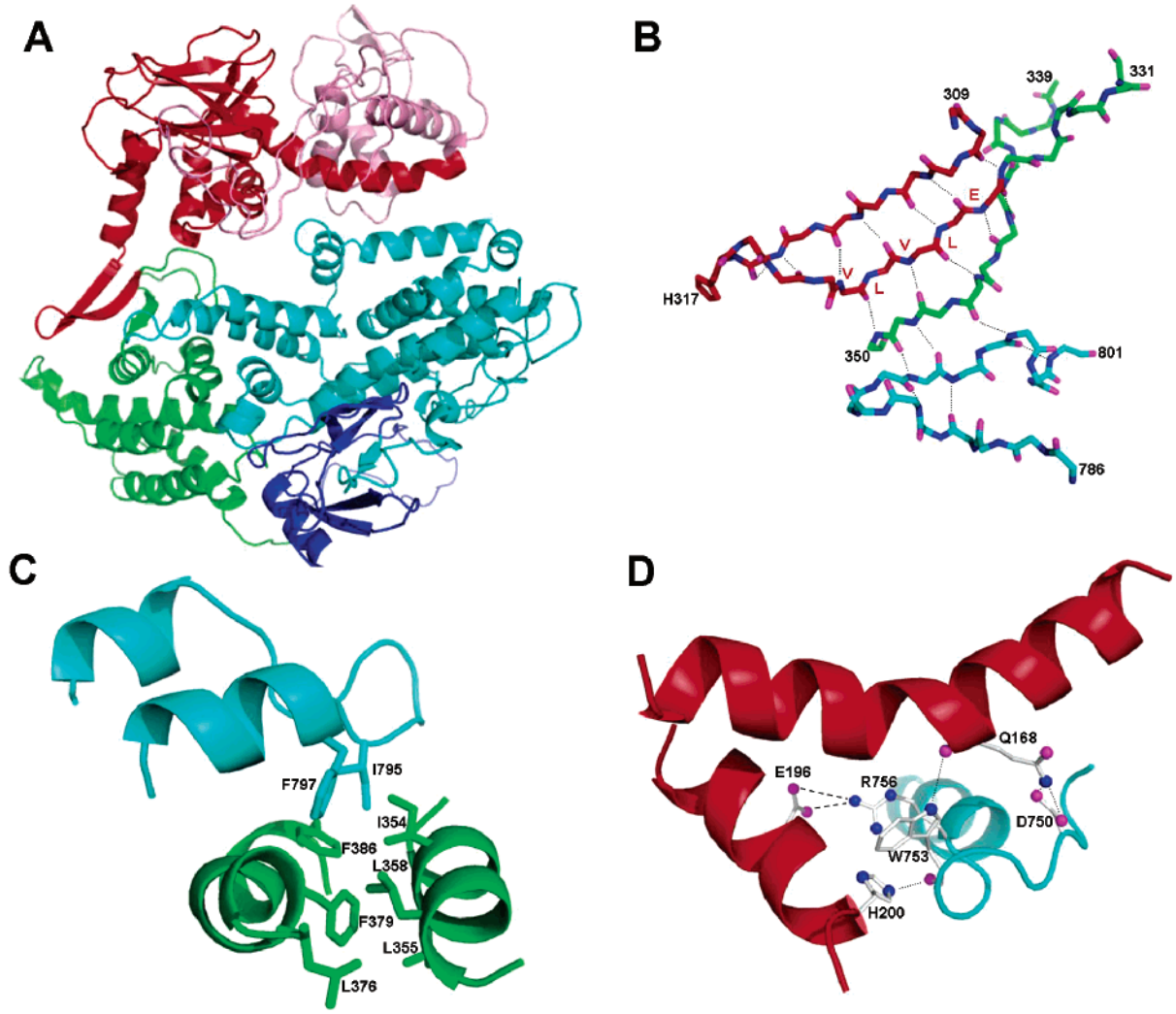

FIGURE 5: Structural model of Epac1. (A) Ribbon diagram of Epac1. The DEP, CBD, REM, RA, and CDC-25 homology domains are colored pink, red, green, blue, and cyan, respectively. (B) Hydrogen bonding network (···) of the switchboard, a five-strand, β-sheet-like structure formed by the C-terminus of CBD (red), the N-terminus of the REM domain (green), and the loop of the helical hairpin of the catalytic core (cyan). (C) Hydrophobic core formed by the C-terminal helix of the helical hairpin of the catalytic core (cyan) and the REM domain (green). (D) Interactions between CBD and CDC-25 homology domains of Epac1. Hydrogen bonding and ionic interactions are shown as dotted and dashed lines, respectively.

and is pivotal for the activation of Epac by cAMP (*29*, *37*, *38*). On the basis of extensive structural, biochemical, and biophysical studies by Bos and Wittinghofer groups, it was proposed that regulation of Epac is dictated by the equilibrium between an inactive and an active state. In the absence of cAMP, Epac exists mostly in the inactive states, in which the lid region, particularly the conserved VLVLE motif, interacts with the catalytic domain and prevents the interaction between Epac and Rap. Binding of cAMP to Epac leads to a conformational change that allows the lid/VLVLE motif to move away from the catalytic core and closer to the cAMP binding pocket to interact directly with cAMP and consequently releases the inhibitory effect of the VLVLE and permits the binding of Rap (*38*). The crystal structure of full-length Epac2 in its inactive, ligand-free state verified the existence of the lid region as part of the switchboard, a five-strand, β-sheet-like structure formed by the C-terminus of CBD, the N-terminus of the REM domain, and the loop of the helical hairpin of the catalytic core (*18*). However, the lid/VLVLE motif is not in the form of a helix as in the case of PKA, nor does the lid/VLVLE motif interact directly with the catalytic core as originally proposed (*38*). To further elucidate the mechanism of Epac activation, we carefully analyzed the structural and sequence homology between Epac and PKA at the lid region. As shown in Figure 6B, although the lid region is not conserved in sequence among all CBD proteins, there is significant sequence homology between Epac and the first cAMP binding domain of the type I regularity subunit of PKA (PKA-RI) in this specific region. Interestingly, while the lid regions of Epac and PKA-RI are similar in sequence, the secondary structure components at this region are different between Epac and PKA-RI. The lid of Epac assumes a β-sheet structure. On the other hand, the lid of PKA-RI is helical both in the presence and in the absence of cAMP (*16*, *39*) (Figure 6B). In fact, the corresponding lid regions of all known CBD proteins except Epac exist as helical structures, although they may differ in their three-dimensional arrangement (*40*). On the basis of these comparative analyses, we proposed the following based on a previously suggested model by Rehemann et al. (*18*, *37*, *38*). In the absence of cAMP, the regulatory and catalytic regions of Epac are held together by the switchboard to keep the CBD in the proximity of the catalytic core to prevent the binding of Rap. The lid/VLVLE motif is anchored and

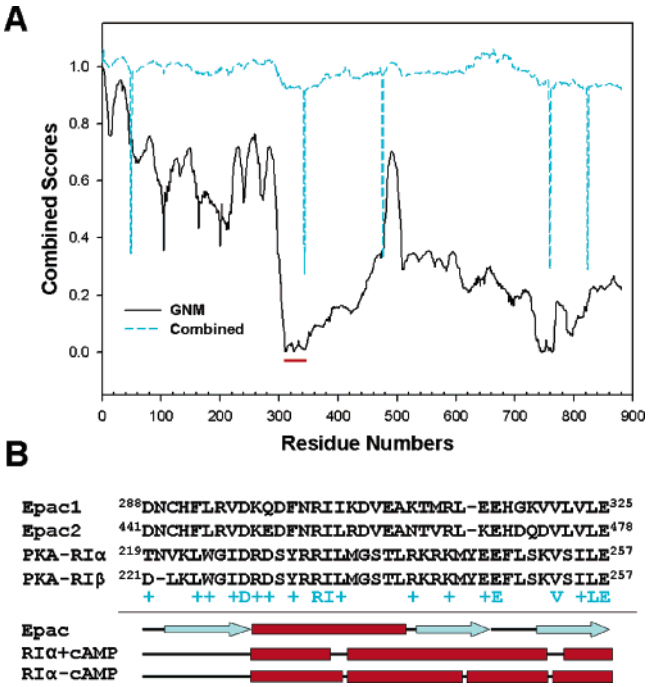

FIGURE 6: Structure and sequence analyses of the lid region of Epac. (A) Hinge prediction results of the Epac1 structure derived from analysis using the HingeMaster server (http://molmovdb.org). The solid black line shows the Gaussian Network Model (GNM) first normal mode displacement score. Minima correspond to hinges. The cyan dashed line shows the combined predictor score using algorithm combines FlexOracle, TLSMD, StoneHinge, and NSHP hinge predictors. Minima correspond to hinges. The red bar highlights the lid region of Epac1. (B) Primary sequence and secondary structure alignments of the lid regions of human Epac and PKA-RI proteins. Secondary structures for Epac and PKA-RI are assigned using X-ray crystal structures 2BYV, 1RGS, and 1RL3.

stabilized by the N-terminus of REM in a three-strand β-sheet structure as part of the switchboard. Binding of cAMP drags the highly conserved PBC in the direction of the cAMP and reorients helix B, tethered to the PBC by a hydrophobic hinge, toward the β-barrel of the CBD. This hinge movement pulls β-strand 1 away from strands 2 and 3 of the three-strand β-sheet of the switchboard. We further predict that the removal of β-strand 1 from the rest of the β-sheet enables it to switch to an α-helix, which folds back to the β-barrel and interacts directly with cAMP to form the base of the cAMP-binding pocket. The net conformational changes induced upon cAMP binding result in an open and active Epac conformation, in which the reorientation of the CBD/DEP relative to the rest of the Epac molecule relieves the catalytic core from the inhibitory contact imposed by the CBD. This transition between the closed/inactive and open/active Epac conformations induced by cAMP has been experimentally demonstrated by an apparent cAMP-induced decrease in the extent of fluorescence resonance energy transfer between enhanced cyan fluorescent protein and citrine fused to the N- and C-termini of Epac1, respectively (*41*).

DISCUSSION

The cAMP-binding domain, conserved from bacteria to humans, is an ancient structural module that acts as a molecular switch for controlling various biological functions. While CBD is a highly conserved and compact structural entity, the functionalities that it regulates vary from DNA binding in the cAMP receptor protein and protein phosphorylation in PKA to membrane potential in cyclic nucleotide-regulated ion channels. The Epac family proteins represent the newest members of the CBD-containing proteins. Unlike PKA, the classic eukaryotic intracellular cAMP receptor, Epac proteins are encoded by single polypeptide chains with the CBD being covalently linked to the catalytic domain, the guanine nucleotide exchange factor domain (*1*, *2*). On the other hand, CBD acts as an inhibitory unit for the catalytic component in both PKA and Epac in the ligand-free state, and cAMP binding leads to the activation of both proteins. One important question that remains to be answered is whether similar structural mechanisms are employed by the CBD during the activation of Epac and PKA.

Extensive biochemical and structural analyses of PKA, particularly the crystal structures of the cAMP-bound regulatory subunit and a partial PKA holoenzyme complex, have revealed a clear picture regarding the interactions between CBD and the catalytic subunit and a detailed mechanism of activation of PKA by cAMP (*16*, *17*). In the PKA holoenzyme complex of RIα(91−244):C, CBD-A of RIα(91−244) makes extensive contact with the C subunit. The B and C helices of CBD-A snap into a single extended helix that is anchored and stabilized by the catalytic subunit, in particular, the activation loop. The PBC is stretched away from the β-barrel to interact directly with the G helix of the C subunit in the complex (*17*). Activation of the PKA holoenzyme, initiated by the binding of cAMP to the R subunit, is accompanied by widespread conformational changes in the R subunit, demonstrated extensively by X-ray crystallographic analyses (*16*, *17*) and biophysical studies in solution (*19*). Binding of cAMP results in the retraction of the PBC in the direction of the cAMP-binding pocket and global reorientation of the subhelical domain of CBD-A. The pivot motion around the hydrophobic hinge dislodges the single extended B/C helix and, subsequently, the inhibitor sequence from the docking site on the C subunit. In the absence of stabilization and anchoring effects of the C subunit, the B/C helix bends in the middle to form two individual helices with the C helix portion folding back onto the β-barrel to form the lid of the cAMP-binding pocket. These extensive cAMP-induced conformational changes eventually cause the dissociation of the PKA holoenzyme.

Since the structure of cAMP-bound Epac in its active state is not currently available, we decided to apply H−D exchange analysis in investigating the conformational and dynamic changes associated with Epac1 activation. Amide H−D exchange has been used extensively to analyze structural dynamics and conformational changes in proteins as the rate at which an amide proton exchanges with the solvent is largely determined by the flexibility and motion around the exchanging proton. To our surprise, unlike PKA, no significant changes in overall secondary structure and structural dynamics, as measured by FT-IR and the rate of H−D exchange, respectively, were observed for Epac1 between cAMP-bound and ligand-free state. These results suggest that Epac1 activation does not involve significant changes in the amount of exposed surface areas as in the case of PKA activation and conformational changes induced by cAMP in Epac1 are most likely local such as hinge motion. These conclusions are consistent with previous biochemical studies as well as the recently determined ligand-

free Epac2 structure (*18*, *29*, *38*). In its autoinhibited state, there is only one direct contact point between the CBD and catalytic core of Epac, described as the "ionic latch". Because of its proximity to the Rap1-binding surface, this ionic latch is believed to be responsible for the inhibitory effect exerted by the CBD on the catalytic activity. Interestingly, the key Arg residue involved in ionic interactions with the CBD in Epac2 is not conserved and replaced with a tryptophan in Epac1, which instead forms hydrogen bonds with the CBD so that the overall structure and function of the ionic latch are preserved in Epac1 (Figure 5D). The CBD is anchored to the catalytic core indirectly by the REM domain through the so-called switchboard, which is a five-strand β-sheet-like structure that consists of the C-terminal lid of the CBD, the N-terminus of the REM domain, and the hairpin of the catalytic core (*18*). The first part of the switchboard, corresponding to the C-terminus of CBD, described as the lid region (B and C helices) of the cAMP binding pocket in PKA, has been suggested to play a critical role in the activation of Epac. On the other hand, the second part of the switchboard, including the N-terminus of the REM domain and the hairpin of the catalytic core, functions to anchor the CBD but most likely does not play important roles during activation of Epac by cAMP, as it has been demonstrated that the isolated CBD half, cleaved between the CBD and REM domains, can completely inhibit the catalytic activity of the GEF half and this inhibition is relieved in response to cAMP binding just like in intact Epac1 (*29*).

The cAMP-free Epac2 structure reveals an unexpected observation. Despite the fact that the lid region of Epac2 and PKA share extensive sequence homology, the corresponding c helix of PKA-RI CBD-A in Epac actually forms the β-strand of the switchboard. In light of this substantial divergence of the lid structure between Epac and PKA, we performed an in-depth comparative sequence and structure analysis of Epac and PKA, and our study leads to a refined model of Epac activation, in which upon binding of cAMP β-strand 1 breaks away from strands 2 and 3 of the three-strand β-sheet of the switchboard, folds back as an α-helix toward the β-barrel, and interacts directly with cAMP to form the base of the cAMP-binding pocket. This localized hinge motion coupled with a switch of the secondary structure of the lid reorients the GEF domain relative to CBD that leads to the ultimate exposure of the catalytic core of Epac for the access of Rap GTPase and, therefore, the activation of Epac. This model is based on the initial model proposed by Rehmann and colleagues (*18*, *37*) and supported by several lines of evidence. First, secondary structure prediction based on several most commonly used algorithms all predicted α-helical structure, instead of a β-strand for the Epac lid region. Second, the corresponding homologous regions of all other known CBD proteins all exist as helical structures despite the fact they may differ in the three-dimensional arrangement (*40*). The unique β-strand structure observed in Epac is most likely due to the stabilization effect provided by strands 2 and 3 of the three-strand β-sheet of the switchboard. In addition, replacing the conserved VLVLE motif in strand 2 with high-helical propensity amino acid side chains such as alanines results in the constitutive activation of Epac (*38*). It is conceivable that these high-helical propensity amino acid substitutions may disrupt the three-strand β-sheet structure, destabilize the interactions between strands 1 and 2, and consequently allow the lid (strand 1) to switch back to a helix because of its natural helical-forming potential. Finally, our model also suggests that while the detailed structural configurations may differ, the same underlying principal is employed by CBDs to control a diverse array of functionalities in different CBD proteins, as demonstrated in the cAMP receptor protein, PKA, and cyclic nucleotide-regulated ion channel systems (*16*, *17*, *42*, *43*).

ACKNOWLEDGMENT

We thank Dr. James C. Lee for the use of the FT-IR instrument and Dr. R. Bryan Sutton for advice in structural modeling.

NOTE ADDED AFTER ASAP PUBLICATION

This paper was published ASAP on December 5, 2006 with incorrect data in the caption of Figure 2. The correct version was reposted on December 5, 2006.

REFERENCES

1. de Rooij, J., Zwartkruis, F. J., Verheijen, M. H., Cool, R. H., Nijman, S. M., Wittinghofer, A., and Bos, J. L. (1998) Epac is a Rap1 guanine-nucleotide-exchange factor directly activated by cyclic AMP, *Nature 396*, 474−477.
2. Kawasaki, H., Springett, G. M., Mochizuki, N., Toki, S., Nakaya, M., Matsuda, M., Housman, D. E., and Graybiel, A. M. (1998) A family of cAMP-binding proteins that directly activate Rap1, *Science 282*, 2275−2279.
3. Ozaki, N., Shibasaki, T., Kashima, Y., Miki, T., Takahashi, K., Ueno, H., Sunaga, Y., Yano, H., Matsuura, Y., Iwanaga, T., Takai, Y., and Seino, S. (2000) cAMP-GEFII is a direct target of cAMP in regulated exocytosis, *Nat. Cell Biol. 2*, 805−811.
4. Seino, S., and Shibasaki, T. (2005) PKA-dependent and PKA-independent pathways for cAMP-regulated exocytosis, *Physiol. Rev. 85*, 1303−1342.
5. Maillet, M., Robert, S. J., Cacquevel, M., Gastineau, M., Vivien, D., Bertoglio, J., Zugaza, J. L., Fischmeister, R., and Lezoualćh, F. (2003) Crosstalk between Rap1 and Rac regulates secretion of sAPPα, *Nat. Cell Biol. 5*, 633−639.
6. Rangarajan, S., Enserink, J. M., Kuiperij, H. B., de Rooij, J., Price, L. S., Schwede, F., and Bos, J. L. (2003) Cyclic AMP induces integrin-mediated cell adhesion through Epac and Rap1 upon stimulation of the β2-adrenergic receptor, *J. Cell Biol. 160*, 487−493.
7. Enserink, J. M., Price, L. S., Methi, T., Mahic, M., Sonnenberg, A., Bos, J. L., and Tasken, K. (2004) The cAMP-Epac-Rap1 pathway regulates cell spreading and cell adhesion to laminin-5 through the $\alpha 3\beta 1$ integrin but not the $\alpha 6\beta 4$ integrin, *J. Biol. Chem. 279*, 44889−44896.
8. Cullere, X., Shaw, S. K., Andersson, L., Hirahashi, J., Luscinskas, F. W., and Mayadas, T. N. (2005) Regulation of vascular endothelial barrier function by Epac, a cAMP-activated exchange factor for Rap GTPase, *Blood 105*, 1950−1955.
9. Kooistra, M. R., Corada, M., Dejana, E., and Bos, J. L. (2005) Epac1 regulates integrity of endothelial cell junctions through VE-cadherin, *FEBS Lett. 579*, 4966−4972.
10. Kiermayer, S., Biondi, R. M., Imig, J., Plotz, G., Haupenthal, J., Zeuzem, S., and Piiper, A. (2005) Epac activation converts cAMP from a proliferative into a differentiation signal in PC12 cells, *Mol. Biol. Cell 16*, 5639−5648.
11. Mei, F. C., Qiao, J., Tsygankova, O. M., Meinkoth, J. L., Quilliam, L. A., and Cheng, X. (2002) Differential signaling of cyclic AMP: Opposing effects of exchange protein directly activated by cyclic AMP and cAMP-dependent protein kinase on protein kinase B activation, *J. Biol. Chem. 277*, 11497−11504.
12. Wang, Z., Dillon, T. J., Pokala, V., Mishra, S., Labudda, K., Hunter, B., and Stork, P. J. (2006) Rap1-Mediated Activation of Extracellular Signal-Regulated Kinases by Cyclic AMP Is Dependent on the Mode of Rap1 Activation, *Mol. Cell. Biol. 26*, 2130−2145.

13. Dodge-Kafka, K. L., Soughayer, J., Pare, G. C., Carlisle Michel, J. J., Langeberg, L. K., Kapiloff, M. S., and Scott, J. D. (2005) The protein kinase A anchoring protein mAKAP coordinates two integrated cAMP effector pathways, *Nature 437*, 574−578.
14. Taylor, S. S., Buechler, J. A., and Yonemoto, W. (1990) cAMP-dependent protein kinase: Framework for a diverse family of regulatory enzymes, *Annu. Rev. Biochem. 59*, 971−1005.
15. Knighton, D. R., Zheng, J. H., Ten Eyck, L. F., Ashford, V. A., Xuong, N. H., Taylor, S. S., and Sowadski, J. M. (1991) Crystal structure of the catalytic subunit of cyclic adenosine monophosphate-dependent protein kinase, *Science 253*, 407−414.
16. Su, Y., Dostmann, W. R., Herberg, F. W., Durick, K., Xuong, N. H., Ten Eyck, L., Taylor, S. S., and Varughese, K. I. (1995) Regulatory subunit of protein kinase A: Structure of deletion mutant with cAMP binding domains, *Science 269*, 807−813.
17. Kim, C., Xuong, N. H., and Taylor, S. S. (2005) Crystal structure of a complex between the catalytic and regulatory (RIα) subunits of PKA, *Science 307*, 690−696.
18. Rehmann, H., Das, J., Knipscheer, P., Wittinghofer, A., and Bos, J. L. (2006) Structure of the cyclic-AMP-responsive exchange factor Epac2 in its auto-inhibited state, *Nature 439*, 625−628.
19. Yu, S., Mei, F. C., Lee, J. C., and Cheng, X. (2004) Probing cAMP-dependent protein kinase holoenzyme complexes Iα and IIβ by FT-IR and chemical protein footprinting, *Biochemistry 43*, 1908−1920.
20. Mei, F. C., and Cheng, X. D. (2005) Interplay between exchange protein directly activated by cAMP (Epac) and microtubule cytoskeleton, *Mol. Biosyst. 1*, 325−331.
21. Dong, A., and Caughey, W. S. (1994) Infrared methods for study of hemoglobin reactions and structures, *Methods Enzymol. 232*, 139−175.
22. Dong, A., Malecki, J. M., Lee, L., Carpenter, J. F., and Lee, J. C. (2002) Ligand-induced conformational and structural dynamics changes in *Escherichia coli* cyclic AMP receptor protein, *Biochemistry 41*, 6660−6667.
23. Jung, C. (2000) Insight into protein structure and protein-ligand recognition by Fourier transform infrared spectroscopy, *J. Mol. Recognit. 13*, 325−351.
24. Susi, H., and Byler, D. M. (1986) Resolution-enhanced Fourier transform infrared spectroscopy of enzymes, *Methods Enzymol. 130*, 290−311.
25. Dong, A., Huang, P., and Caughey, W. S. (1990) Protein secondary structures in water from second-derivative amide I infrared spectra, *Biochemistry 29*, 3303−3308.
26. Barksdale, A. D., and Rosenberg, A. (1982) Acquisition and interpretation of hydrogen exchange data from peptides, polymers, and proteins, *Methods Biochem. Anal. 28*, 1−113.
27. Marti-Renom, M. A., Stuart, A. C., Fiser, A., Sanchez, R., Melo, F., and Sali, A. (2000) Comparative protein structure modeling of genes and genomes, *Annu. Rev. Biophys. Biomol. Struct. 29*, 291−325.
28. Qiao, J., Mei, F. C., Popov, V. L., Vergara, L. A., and Cheng, X. (2002) Cell cycle dependent subcellular localization of exchange factor directly activated by cAMP, *J. Biol. Chem. 277*, 26581−26586.
29. de Rooij, J., Rehmann, H., van Triest, M., Cool, R. H., Wittinghofer, A., and Bos, J. L. (2000) Mechanism of regulation of the Epac family of cAMP-dependent RapGEFs, *J. Biol. Chem. 275*, 20829−20836.
30. Kraemer, A., Rehmann, H. R., Cool, R. H., Theiss, C., de Rooij, J., Bos, J. L., and Wittinghofer, A. (2001) Dynamic interaction of cAMP with the Rap guanine-nucleotide exchange factor Epac1, *J. Mol. Biol. 306*, 1167−1177.
31. Kraemer, A., Rehmann, H. R., Cool, R. H., Theiss, C., de Rooij, J., Bos, J. L., and Wittinghofer, A. (2001) Dynamic interaction of cAMP with the Rap guanine-nucleotide exchange factor Epac1, *J. Mol. Biol. 306*, 1167−1177.
32. Blout, E. R., de Lozé, C., and Asadourian, A. (1961) *J. Am. Chem. Soc. 83*, 1895−1900.
33. Kim, K. S., Fuchs, J. A., and Woodward, C. K. (1993) Hydrogen exchange identifies native-state motional domains important in protein folding, *Biochemistry 32*, 9600−9608.
34. de Jongh, H. H., Goormaghtigh, E., and Ruysschaert, J. M. (1995) Tertiary stability of native and methionine-80 modified cytochrome c detected by proton-deuterium exchange using on-line Fourier transform infrared spectroscopy, *Biochemistry 34*, 172−179.
35. Li, J., Cheng, X., and Lee, J. C. (2002) Structure and dynamics of the modular halves of *Escherichia coli* cyclic AMP receptor protein, *Biochemistry 41*, 14771−14778.
36. Flores, S., Echols, N., Milburn, D., Hespenheide, B., Keating, K., Lu, J., Wells, S., Yu, E. Z., Thorpe, M., and Gerstein, M. (2006) The Database of Macromolecular Motions: New features added at the decade mark, *Nucleic Acids Res. 34*, D296−D301.
37. Rehmann, H., Prakash, B., Wolf, E., Rueppel, A., de Rooij, J., Bos, J. L., and Wittinghofer, A. (2003) Structure and regulation of the cAMP-binding domains of Epac2, *Nat. Struct. Biol. 10*, 26−32.
38. Rehmann, H., Rueppel, A., Bos, J. L., and Wittinghofer, A. (2003) Communication between the regulatory and the catalytic region of the cAMP-responsive guanine nucleotide exchange factor Epac, *J. Biol. Chem. 278*, 23508−23514.
39. Wu, J., Brown, S., Xuong, N. H., and Taylor, S. S. (2004) RIα subunit of PKA: A cAMP-free structure reveals a hydrophobic capping mechanism for docking cAMP into site B, *Structure 12*, 1057−1065.
40. Berman, H. M., Ten Eyck, L. F., Goodsell, D. S., Haste, N. M., Kornev, A., and Taylor, S. S. (2005) The cAMP binding domain: An ancient signaling module, *Proc. Natl. Acad. Sci. U.S.A. 102*, 45−50.
41. DiPilato, L. M., Cheng, X., and Zhang, J. (2004) Fluorescent indicators of cAMP and Epac activation reveal differential dynamics of cAMP signaling within discrete subcellular compartments, *Proc. Natl. Acad. Sci. U.S.A. 101*, 16513−16518.
42. McKay, D. B., and Steitz, T. A. (1981) Structure of catabolite gene activator protein at 2.9 Å resolution suggests binding to left-handed B-DNA, *Nature 290*, 744−749.
43. Clayton, G. M., Silverman, W. R., Heginbotham, L., and Morais-Cabral, J. H. (2004) Structural basis of ligand activation in a cyclic nucleotide regulated potassium channel, *Cell 119*, 615−627.

BI061701X